

Pulsed Saturation of the Standard Two-Pool Model for Magnetization Transfer. Part II: The Transition to Steady State

GUNTHER HELMS,^{1,2} HENNING DATHE,³ GISELA E. HAGBERG⁴

¹ Section on Experimental Radiology, Department of Diagnostic Radiology, University of Tübingen, Germany

² MR Centrum, Department of Clinical Neuroscience, Karolinska Institutet, Stockholm, Sweden

³ Biomechanics Research Group, Department of Orthodontics, University of Göttingen, Germany

⁴ Laboratory of Functional Neuroimaging, Fondazione Santa Lucia IRCCS, Rome, Italy

ABSTRACT: The transition of the tissue signal to steady state under periodic selective saturation of macromolecular magnetization can be observed by single-shot echo-planar imaging. The general solution for a two-pool system with linear exchange kinetics contains two transient components. The rapid minor transient causes an initial delay of the transition for fast pulse repetition (*PR*) and weak saturation. The slow major transient combines progressive direct saturation and transferred saturation. Its *PR*-dependence provides similar information as the steady state, but is less sensitive to direct saturation and fitting errors. Sampling at different *PR* allows to quantify all system parameters. © 2004 Wiley Periodicals, Inc. Concepts Magn Reson Part A 21A: 50–62, 2004

KEY WORDS: magnetization transfer; pulsed saturation; transient behavior; quantification; human brain

INTRODUCTION

Magnetization transfer (MT) contrast (*I*) is created by selectively saturating the “invisible” magnetization of

Received 14 August 2003; revised 09 December 2003; accepted 09 December 2003

Correspondence to: Gunther Helms, Universitätsklinikum Tübingen, Abt. Radiologische Diagnostik, Sektion für experimentelle Radiologie, Hoppe-Seyler-Str. 3, DE-72076 Tübingen, Germany; E-mail: gunther.helms@cns.ki.se

Concepts in Magnetic Resonance Part A, Vol. 21A(1) 50–62 (2004)
Published online in Wiley InterScience (www.interscience.wiley.com). DOI 10.1002/cmra.20005

© 2004 Wiley Periodicals, Inc.

macromolecules and can be observed as attenuation of the “free” water signal. On clinical MR systems, the saturation is often accomplished by selective radio-frequency (RF) pulses applied at a frequency outside their excitation bandwidth (MT-pulses). Pulsed saturation and slice excitation are interleaved in common MT imaging sequences, thus creating steady state conditions. In contrast, the transition to steady state due to repetitive application of the MT-pulse can be measured by single-shot read-out of the longitudinal magnetization (2).

In the first part, we introduced the terminology and developed a theoretical framework to describe the standard two-pool model of MT undergoing repetitive

pulsed saturation. We provided an approximation for MT in tissue that is based on the observation that the transfer fast compared to the relaxation process. Thus, the dependence of the steady state on the repetition period (*PR*) of the MT-pulses can be explained by an early phase of rapid transfer re-establishing kinetic equilibrium, and a late phase of slow relaxation of both pools by the weighted average of the individual relaxation rates.

In the second part, we discuss the transition of the MT system into the steady state. This article provides the general analytic solution of the transient behavior for arbitrary saturation of the pools. Trajectories of the evolving saturation in the plane of longitudinal saturation provide the key for understanding of the transition behavior (3). The theory is applied to in vivo MT experiments on human brain. The transition has distinct advantages over the steady state for quantitative evaluation because it is less prone to errors than the steady state alone. Quantification of the MT-model is possible by a global fit of the transitions at short and long *PR*.

GENERAL SOLUTION OF THE TRANSITION TO STEADY STATE

Solving the Recursion

In the first article, the recursion of pulsed saturation and subsequent free evolution during *PR* (Eq. [I-27]) has been described in matrix form for the saturation vector $\boldsymbol{\eta}$ by arbitrary degrees of saturation for each pool (δ_f, δ_m) and by the transfer matrix (\mathbf{T}). The n -th recursion can be written in generalized form as

$$\boldsymbol{\eta}^n = \mathbf{A}\boldsymbol{\eta}^{n-1} + \mathbf{b}, \quad [1]$$

where

$$\mathbf{A} = \mathbf{T} \begin{pmatrix} 1 - \delta_f & 0 \\ 0 & 1 - \delta_m \end{pmatrix} \quad [2]$$

$$\mathbf{b} = \mathbf{T} \begin{pmatrix} \delta_f \\ \delta_m \end{pmatrix}. \quad [3]$$

Equation [1] is solved by

$$\boldsymbol{\eta}^n = \boldsymbol{\eta}^\infty + \mathbf{A}^n(\boldsymbol{\eta}^0 - \boldsymbol{\eta}^\infty), \quad [4]$$

where $\boldsymbol{\eta}^0$ denotes an arbitrary initial state, and $\boldsymbol{\eta}^\infty$ the steady state:

$$\boldsymbol{\eta}^\infty = (\mathbf{I} - \mathbf{A})^{-1}\mathbf{b}. \quad [5]$$

\mathbf{I} is the (2×2) unity matrix. In the following, we discuss the standard situation of the initial state being equilibrium magnetization: $\boldsymbol{\eta}^0 = (0 \ 0)^T$. This case is considerably simplified by use of $\boldsymbol{\eta}$. From

$$\boldsymbol{\eta}^n = (\mathbf{I} - \mathbf{A}^n)\boldsymbol{\eta}^\infty = (\mathbf{I} - \mathbf{A}^n)(\mathbf{I} - \mathbf{A})^{-1}\mathbf{b} \quad [6]$$

one verifies immediately the first steps of the recursion: $\boldsymbol{\eta}^1 = \mathbf{b}$ and $\boldsymbol{\eta}^2 = \mathbf{b} + \mathbf{A}\mathbf{b}$. Further powers of \mathbf{A} can be calculated by recursively applying the Cayley-Hamilton theorem that \mathbf{A} satisfies its own characteristic equation:

$$\mathbf{A}^2 - (\mu_+ + \mu_-)\mathbf{A} + \mu_+\mu_-\mathbf{I} = \mathbf{0}. \quad [7]$$

Thus, \mathbf{A}^2 is expressed as linear combination of \mathbf{A} and \mathbf{I} . Because \mathbf{A} is a 2×2 matrix, trace and determinant of \mathbf{A} (see Eqs. [13, 14]) have been expressed by the eigenvalues of \mathbf{A} ,

$$\begin{aligned} \mu_{+/-} &= \frac{1}{2} [(1 - \delta_f)T_{ff} + (1 - \delta_m)T_{mm}] \\ &\pm \frac{1}{2} \sqrt{[(1 - \delta_f)T_{ff} - (1 - \delta_m)T_{mm}]^2 + 4(1 - \delta_f)(1 - \delta_m)T_{fm}T_{mf}}. \end{aligned} \quad [8]$$

The following formula can be proven by induction:

$$\mathbf{A}^n = \frac{\mu_+^n - \mu_-^n}{\mu_+ - \mu_-} \mathbf{A} - \mu_+\mu_- \frac{\mu_+^{n-1} - \mu_-^{n-1}}{\mu_+ - \mu_-} \mathbf{I}. \quad [9]$$

Replacing \mathbf{A}^n in Eq. [4] yields

$$\boldsymbol{\eta}^n = \left[\left(1 + \mu_+\mu_- \frac{\mu_+^{n-1} - \mu_-^{n-1}}{\mu_+ - \mu_-} \right) \mathbf{I} - \frac{\mu_+^n - \mu_-^n}{\mu_+ - \mu_-} \mathbf{A} \right] \boldsymbol{\eta}^\infty. \quad [10]$$

Because the macromolecules cannot be measured directly, it is beneficial to choose a parameterization that represents η_f by parameters than can be observed in the water signal. By replacing $\mathbf{A}\boldsymbol{\eta}^\infty = \boldsymbol{\eta}^\infty - \boldsymbol{\eta}^1$ (Eq. [5]) and sorting for powers of $\mu_{+/-}$ one obtains

$$\begin{aligned} \boldsymbol{\eta}^n = \boldsymbol{\eta}^\infty - \frac{1}{\mu_+ - \mu_-} & \left([(1 - \mu_-)\boldsymbol{\eta}^\infty - \boldsymbol{\eta}^1] \mu_+^n \right. \\ & \left. - [(1 - \mu_+)\boldsymbol{\eta}^\infty - \boldsymbol{\eta}^1] \mu_-^n \right). \end{aligned} \quad [11]$$

This general solution shows that the transition to steady state actually consists of two transients $\mu_{+/-}$, namely the eigenvalues of \mathbf{A} . Together with $\boldsymbol{\eta}^\infty$ and $\boldsymbol{\eta}^1$, these six parameters are equivalent to the saturation factors, the kinetic and relaxation rates. In principle, only four of them can be determined from a one

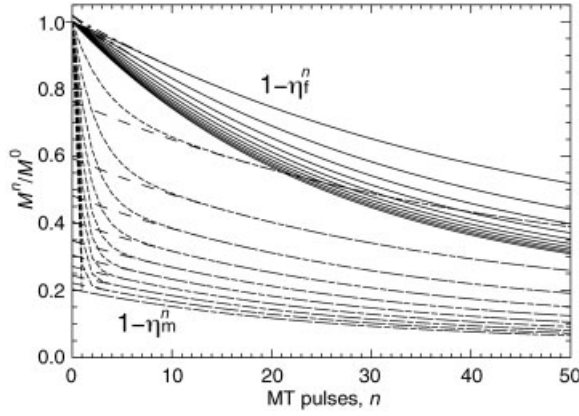


Figure 1 Biexponential transition of the water pool and macromolecular pool. The normalized magnetizations ($M_m/M_m^0 = 1 - \eta_m$, $M_f/M_f^0 = 1 - \eta_f$) are shown (solid lines). Curves were calculated for WM at a short PR of 5 ms for macromolecular saturation ($\delta_m = 1\%$, 10% , 20% , \dots , 100% , and $\delta_f = 1\%$) using the parameters from Ref. (4). The components of the major transient have been extrapolated to $PR = 0$ (dashed for M_m/M_m^0 , dashed-dotted for M_f/M_f^0) to show the components of the minor transient.

transition with a certain PR . Hence, the PR -dependence has to be exploited to obtain a complete characterization of the all system parameters.

For a homogeneous liquid the transition shows one component (Eq. [I-21]). The occurrence of a second transient results from the presence of a second pool. Figure 1 shows the start of the transition for both pools in WM at the shortest experimental PR value (5 ms). As in part I, simulations were performed using the parameters for bovine gray and white matter (GM/WM) as determined *ex vivo* at 37°C (4). The transition of the macromolecular pool (dashed curves) is strongly influenced by the minor transient. In this pool, the amplitude of the minor transient is large enough to visualize that this transition gets shorter when δ_m is increased. Because the amplitude of the minor transient is much smaller in the water pool, μ_- can only be observed if the component is visible in a sufficient number of points at the start of the transition. Already $\mu_- = 0.5$ can already be considered unobservable because the component has decayed by 88% at the third iteration. Because the amplitude of the rapid transition component is negative, it may still be observed indirectly by an overshoot of amplitude of the slow component exceeding the reference signal.

The physical origin of this component is illustrated in Figure 2. The vector representation shows the trajectories of saturation, transfer, and relaxation in the η -plane at short PR when the MT is not fully accomplished. The construction has been explained in part I.

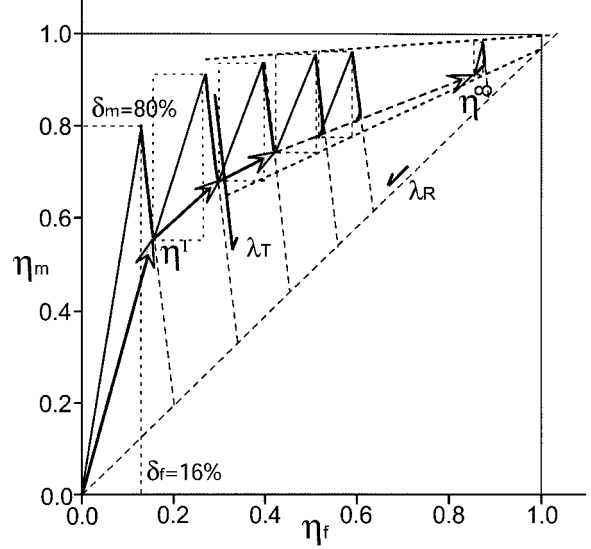


Figure 2 Approach to steady state in the η -plane at short PR . The major transition follows the eigenvector of μ_+ . The additional saturation in η_m is built up during the first iterations. Then the steady state η^∞ is approached on a straight line given by the eigenvector of μ_+ (Eq. [25]). The construction from saturation transfer and relaxation was explained in Figure 2 of part I.

Here, the steady state saturation is larger for macromolecules than for water. It may take a couple of iterations to build up the additional saturation of the macromolecular pool, just like in a homogeneous system (Eq. [I-23]). This delays the increase of saturation of the free pool, where the rapid transient thus appears with negative amplitude. The amplitude of the minor transient is much smaller in the free water than in the macromolecules, because the macromolecular ratio is small in tissue. The same interrelation has been discussed in part I for saturation transfer. After the excess saturation of the macromolecules has been built up, both pools slowly approach the steady state with μ_+ .

PR -Dependence of the Transients

Because $\mu_{+/-}$ can be expressed by the invariants of \mathbf{A} ,

$$\mu_{+/-} = \frac{1}{2} \text{tr } \mathbf{A} \pm \frac{1}{2} \sqrt{(\text{tr } \mathbf{A})^2 - 4 \det \mathbf{A}}, \quad [12]$$

the product and the sum of the two transients have a simple time dependence:

$$\begin{aligned} \mu_- \mu_+ &= \det \mathbf{A} = (1 - \delta_f)(1 - \delta_m) \det \mathbf{T} \\ &= (1 - \delta_f)(1 - \delta_m) E_T E_R \quad [13] \end{aligned}$$

$$\begin{aligned} \mu_+ + \mu_- = \text{tr } \mathbf{A} &= (1 - \delta_f)E_R + (1 - \delta_m)E_T \\ &- T(\delta_m - \delta_f)(E_R - E_T). \quad [14] \end{aligned}$$

Here we used the parameterization of \mathbf{T} that has been introduced in part I (Eq. [I-18]). The trace contains the term of transferred saturation that rapidly increases with λ_T (Eq. [I-7a]) until reaching its maximum at t_{crit} (Eq. [I-11]), and relaxes slowly with λ_R (Eq. [I-7b]) once the pre-equilibrium has been established. Because the difference term does not appear in Eqs. [13] and [14], the transients depend solely on T . For later use, we note that the denominator of (Eq. [I-29]) can be re-written by means of the transients:

$$\begin{aligned} [1 - (1 - \delta_m)E_T][1 - (1 - \delta_f)E_R] \\ + T(\delta_m - \delta_f)(E_T - E_R) \\ = \det(\mathbf{E} - \mathbf{A}) = (1 - \mu_-)(1 - \mu_+). \quad [15] \end{aligned}$$

Figure 3 shows the PR dependence of the transients for varying saturation of macromolecules ($\delta_m = 20\%, 40\%, \dots 100\%$) and $\delta_f = 1\%$. The curves were calculated from Eqs. [12–14]. The minor transient (μ_- , solid lines) closely resembles the transfer component, E_T , and is scaled by $1 - \delta_m$. There are two contributions to the major transient (μ_+ , solid lines): the term of progressive direct saturation, $(1 - \delta_f)E_R$ (Eq. [I-23]) and the transferred saturation that accelerates the transition. Clearly, μ_+ decreases more rapidly in WM than in GM because of the faster relaxation of free water. In WM, the stepwise increase of δ_m results in a larger reduction of μ_+ than in GM, because the macromolecular fraction, and hence the transfer term, are larger. A further small increase of direct saturation (as in Fig. 4 of part I), would result mainly in small negative offset to the curves shown in Figure 3 (not shown). This offset does not change the typical appearance of the PR -dependence, as long as the differential saturation, $\delta_m - \delta_f$, does not become too small. Contrary to the steady state, increasing δ_f to 4% does not lead to a loss of the characteristic features of the curves.

The largest MT reduction of μ_+ is seen for $\delta_m \rightarrow 100\%$. In this case, Eq. [8] yields $\mu_+ = (1 - \delta_f)T_{\text{ff}}$ (Eq. [I-9a]), and thus the PR -dependence becomes biexponential (bold curve in Fig. 3). However, the PR -dependence of μ_+ is generally not biexponential for weaker saturations. This can be seen in the initial slope of the curve for $\delta_m = 20\%$. Equal saturation of the pools ($\delta_m = \delta_f$, dashed curves) yields immediately that $\mu_+ = (1 - \delta_f)E_R$ and $\mu_- = (1 - \delta_m)E_T$: The transitions are decoupled when no transfer takes place during PR . In the limit of $PR \rightarrow 0$, μ_+

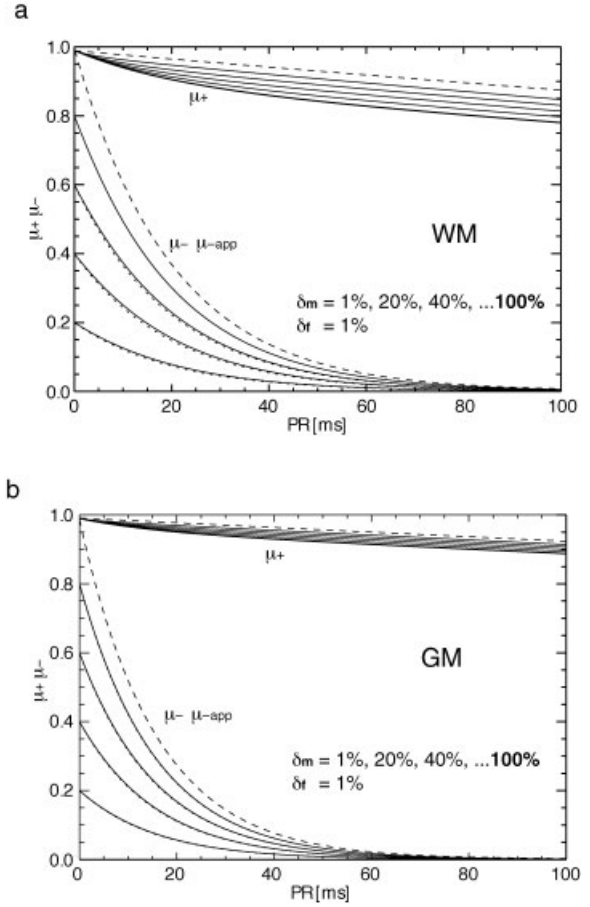


Figure 3 PR -dependence of the major and minor transient in WM (a) and GM (b). The solid curves indicate μ_- and μ_+ for $\delta_m = 20\%, 40\%, \dots 100\%$ and $\delta_f = 1\%$; the dotted curves the approximation by $\mu_{-app} = (1 - \delta_m)E_T$. The monoexponential case of equal saturation without MT ($\delta_m = \delta_f = 1\%$) is indicated by dashed lines. By comparison to the bold curve showing the biexponential μ_+ for $\delta_m = 100\%$ one sees that the PR -dependence of μ_+ is generally not exponential.

approaches $1 - \delta_f$ and μ_- approaches $1 - \delta_m$ because the free evolution is too short for considerable transfer to take place.

We now discuss the transients for the three domain of PR that have been identified in the steady state curves shown in Figure 3 of Part I.

For long PR ($> 5 \lambda_T^{-1}$), the kinetic pre-equilibrium is attained after the rapid transfer component has decayed to zero. According to Eq. [13], $\det \mathbf{A}$ and thus the minor transient have also become zero. In this case, Eq. [11] gives for $n = 0$

$$\eta^\infty = \frac{1}{1 - \mu_+} \eta^1, \quad [16]$$

and the transition thus takes the form

$$\boldsymbol{\eta}^n = \frac{1 - \mu_+^n}{1 - \mu_+} \boldsymbol{\eta}^1 = (1 - \mu_+^n) \boldsymbol{\eta}^\infty. \quad [17]$$

The analogy to partial progressive saturation of a homogeneous liquid (Eqs. [I-22–24]) applies also to the dynamic behavior of pulsed MT at long PR . The major transient is identical to $\text{tr } \mathbf{A}$. This shows that the direct saturation is increased by MT, given by the product of the differential saturation and T :

$$\mu_+ = \text{tr } \mathbf{A} = [1 - \delta_f - T(\delta_m - \delta_f)]E_R. \quad [18]$$

The saturations approach the steady state along the line of pre-equilibrium in the $\boldsymbol{\eta}$ -plane (part I, Fig. 2).

This line is given by that the eigenvectors of \mathbf{T} for the eigenvalue λ_R . In the parameterization of \mathbf{T} (Eq. [I-18]), these eigenvectors are multiples of (\mathbf{T}^{-1}) . Thus, every $\boldsymbol{\eta}^n$ is such an eigenvector, and so is every $\Delta\boldsymbol{\eta}^n = \boldsymbol{\eta}^n - \boldsymbol{\eta}^{n-1}$. From Eqs. [1] and [17] follows that

$$\Delta\boldsymbol{\eta}^n = \mathbf{A}\Delta\boldsymbol{\eta}^{n-1} = \mu_+\Delta\boldsymbol{\eta}^{n-1}. \quad [19]$$

The straight transition implies that the eigenvectors of \mathbf{T} for the eigenvalue λ_R are also eigenvectors of \mathbf{A} for the eigenvalue μ_+ .

For short PR ($< 5 \lambda_T$), an approximation of μ_- can be derived by rearranging the terms under the root in Eq. [8], so that the square root reads

$$\mu_+ - \mu_- = \sqrt{[(1 - \delta_f)E_R - T(\delta_m - \delta_f)(E_R - E_T) - (1 - \delta_m)E_T]^2 - 4(1 - \delta_m)E_T T(\delta_m - \delta_f)(E_R - E_T)}. \quad [20]$$

Because $T \ll 1$ in tissue, linear expansion of the root (similar to Eq. [I-34]) yields

$$\begin{aligned} \mu_+ - \mu_- \cong & [(1 - \delta_f)E_R - T(\delta_m - \delta_f)(E_R - E_T) - (1 - \delta_m)E_T] \\ & \times \left(1 - 2(1 - \delta_m)E_T \frac{T(\delta_m - \delta_f)(E_R - E_T)}{(1 - \delta_f)E_R - T(\delta_m - \delta_f)(E_R - E_T) - (1 - \delta_m)E_T} \right), \quad [21] \end{aligned}$$

and thus

$$\mu_- \cong (1 - \delta_m)E_T \left(1 - \frac{T(\delta_m - \delta_f)(E_R - E_T)}{(1 - \delta_f)E_R - (1 - \delta_m)E_T - T(\delta_m - \delta_f)(E_R - E_T)} \right). \quad [22]$$

Thus it is shown, that μ_- is proportional to $1 - \delta_m$ and decreases rapidly with E_T . The minor transient appears only in the first iterations, when the free pool is still almost unsaturated, and at short PR , when transfer is insignificant. This is the reason why the bound pool is saturated as if the free pool were absent. For further approximation of the transients, we neglect the last factor in Eq. [22]:

$$\mu_{-app} \cong (1 - \delta_m)E_T. \quad [23]$$

This approximation is shown in Figure 3 (dotted lines). Deviations from the exact solution are seen only for $\mu_- < 0.5$, which is difficult to observe in the free water. It seems straightforward to derive the associated μ_{+app} from Eq. [13] or [14]. However, the resulting mono- or biexponential PR -dependence is too simple to describe the experiment sufficiently, because the major transient (unlike the minor transient) can be measured with high accuracy. In addition, simulation shows that large errors appear for short PR , when calculating the steady state using the transients (Eq. [15]). Hence, steady state and

transient would be no longer consistent. With the approximation

$$\mu_{+app} \cong (1 - \delta_f)E_R - T(\delta_m - \delta_f)(E_R - E_T)/(1 - (1 - \delta_m)E_T). \quad [24]$$

Equation [15] remains valid. The divisor in the MT-term, $1 - (1 - \delta_m)E_T$, becomes one in the limit of long PR or $\delta_m \rightarrow 100\%$. When replacing μ_+ by μ_{+app} in Eq. [19], it is rather easy to calculate the approximate eigenvectors for λ_R even at short PR :

$$\mathbf{n}_{+app} \cong \begin{pmatrix} (T - D)(1 - (1 - \delta_m)E_T) \\ T(1 - (1 - \delta_f)E_T) \end{pmatrix} \xrightarrow{PR \rightarrow \infty} \begin{pmatrix} T - D \\ T \end{pmatrix}. \quad [25]$$

Along the line given by \mathbf{n}_{+app} the steady state is approached in the \mathbf{n} -plane in Figure 2. The steady state of the observable water can be written as

$$\frac{M_f^\infty}{M_f^0} = \frac{1 - E_R}{1 - \mu_{+app}} \left[1 + D \frac{\delta_m(E_R - E_T)}{(1 - (1 - \delta_m)E_T)(1 - E_R)} \right]. \quad [26]$$

The main term appears like progressive saturation of a homogeneous sample. The transfer term is determined from the transient and the difference term from the ‘‘mismatch’’ of the actual steady state. In theory, this offers the possibility to determine all system parameters from the free water signal alone, even when the invisible pool cannot be assessed directly. In the first part, we showed that the additional assumption of a small macromolecular pool allows to neglect D . The PR -dependence of the apparent transient, μ_{+app} , is consistent with the apparent saturation defined in Eq. [I-41]. The analogy to progressive partial saturation of a homogeneous sample is thus extended to both the transition and the steady state. Of course, this analogy implies that the minor transient can be neglected, thus requiring sufficient macromolecular saturation.

At very short $PR (\ll \lambda_T^{-1})$, MT becomes insignificant. In the steady state, both pools are strongly saturated at such short PR . After linear expansion in PR , the pools appear decoupled in the transients:

$$\mu_+ \cong (1 - \delta_f)(1 - R_f PR) \xrightarrow{PR \rightarrow 0} 1 - \delta_f \quad [27a]$$

$$\mu_- \cong (1 - \delta_m)(1 - R_m PR) \xrightarrow{PR \rightarrow 0} 1 - \delta_m. \quad [27b]$$

The minor transient describes the buildup of saturation in the macromolecular pool, which mainly depends on δ_m , since $R_m PR$ is small. The PR -dependence by R_f and R_m (Eqs. [I-4a,b]) results directly from the modified Bloch equations (Eq. [I-3]). The second limit results from Eqs. [12–14] when considering that $\text{tr } \mathbf{A} \rightarrow 1 - \delta_f + 1 - \delta_m$ and $\det \mathbf{A} \rightarrow (1 - \delta_f)(1 - \delta_m)$ for $PR \rightarrow 0$.

CALCULATION OF THE PRIMARY KINETIC PARAMETERS FROM λ_T , λ_R , T , AND D

We have shown so far how the observed water signal depends on the parameters λ_T , λ_R , T , and D . In order to quantify the transfer, one has to transform this parameter set into the rate constants of the modified Bloch equation (Eq. [I-3]). The kinetic rate constants can be directly calculated when comparing T_{fm} and T_{mf} in Eqs. [I-8] and [I-16]:

$$k_{fm} = (T - D)(\lambda_T - \lambda_R) \quad [28]$$

$$k_{mf} = \frac{T(1 - T)}{T - D} (\lambda_T - \lambda_R). \quad [29]$$

Thus, one immediately derives the pool size ratio,

$$f = \frac{(T - D)^2}{T(1 - T)}. \quad [30]$$

When using the approximation of fast transfer to express λ_R , λ_T , T , and D (Eqs. [I-13–15]), Eq. [30] is slightly modified. After combining Eqs. [I-14] and [I-15], the transfer term can be written as

$$T = \frac{f}{1 + f} + 2D \left(1 - \frac{f}{1 + f} \right), \quad [31]$$

so one gets

$$f = \frac{T - 2D}{1 - T}. \quad [32]$$

Comparison with Eq. [30] reveals that the small term of D^2 is neglected in Eq. [32] as result of the fast transfer approximation. From Eqs. [28] and [32] one obtains first k_{mf} , and then R_{1f} and R_{1m} from Eqs. [I-15a,b]:

$$k_{mf} = \frac{(T - D)(1 - T)}{T - 2D} (\lambda_T - \lambda_R) \quad [33]$$

$$R_{1f} = D\lambda_T + (1 - D)\lambda_R \quad [34]$$

$$\begin{aligned} R_{1m} &= \lambda_R - D(\lambda_T - \lambda_R)/f \\ &= -\frac{D(1 - T)}{T - 2D}\lambda_T + \frac{T - D - DT}{T - 2D}\lambda_R. \end{aligned} \quad [35]$$

In the first part, we showed that the additional assumption of a small macromolecular pool allows to neglect D . Thus, the number of parameters is reduced by one. This is equivalent to the assumption that the longitudinal relaxation is the same in both pools ($R_{1f} = R_{1m} = \lambda_R$). This can be seen by replacing $D = 0$ in Eqs. [34] and [35]. In this case, the kinetic rate constants are calculated by

$$k_{fm} = T(\lambda_T - \lambda_R) \quad [36]$$

and

$$k_{mf} = (1 - T)(\lambda_T - \lambda_R), \quad [37]$$

where $T \cong f/(1 + f)$ (Eq. [I-39]). By neglecting the minor transient and D in Eq. [26], the dynamics of the progressive saturation of the bulk water is described in analogy to a homogeneous liquid by means of a PR -dependent apparent saturation Eq. ([I-41]).

EXPERIMENTAL

Healthy adult subjects were examined on a 1.5 Tesla clinical MR system (Magnetom Vision, Siemens Medical Solutions, Erlangen, Germany) using the standard circular-polarized head coil. The motion-restricted magnetization was saturated by an equidistant train of band-selective RF -pulses applied at least 1 kHz off-resonance. In order to achieve efficient macromolecular saturation through high pulse power and small frequency offsets, a Gaussian-shaped pulse envelope was chosen. The duration of the MT-pulses was 3.2, 6.4, or 12.8 ms, corresponding to nominal bandwidths (full width at half maximum) of 480, 240, or 120 Hz, respectively. Because of a long recovery period ($TR = 10$ s), the maximum duty cycle (smallest PR) was imposed by the RF power amplifier, but not by specific heat absorption. It hence depended on coil loading (head size) and pulse power.

A single-shot spin-echo echo-planar imaging (EPI) sequence (TE = 50 ms, 5-mm slice thickness, field-of-view 192 mm, 64×64 matrix) was used to read-out the water magnetization in an axial-oblique slice through the *centrum semiovale*. Fat-suppression by a series of four binomial pulses was accommodated in

the final PR interval. The image intensity was evaluated on manually selected regions-of-interest (ROIs) of about 50 pixels in central WM and cortical GM (each ROI corresponded to a tissue volume of about 2.25 ccm). Signal contributions from cerebro-spinal fluid (CSF) were determined from a biexponential fit to a series of 16 single-echo measurements at TEs up to 800 ms.

In order to measure the second transient, MT-pulses of 3.2 ms duration were applied at 4 kHz with a nominal flip angle of 180° at the shortest possible PR of 5 ms.

In order to obtain a strong saturation for the steady state measurements, we chose a long pulse duration (12.8 ms) and large nominal flip angles between 1080° and 1800° . The frequency offset was 1 kHz, which is well outside the band of direct excitation [Fig. 1 of Ref. (5)]. The PR range was between 25 and 1000 ms. The data were corrected for CSF contributions and evaluated by Eq. [I-40].

To achieve a compromise between strong saturation and short PR , 720° pulses of 6.4 ms duration were applied at 1 kHz. The steady state was measured at PR between 8 and 200 ms. The transition to steady state was sampled at short PR of 8, 16, 24 ms and long PR of 100 and 200 ms. Reference measurements were performed between each of those series to account for signal drifts during the experiment.

In order to fit the PR -dependence of μ_{+app} to only five independently determined values of μ_+ , the apparent relaxation rate had to be calculated from the slow component of μ_+ measured at long PR (Eq. [18]):

$$\lambda_R = \frac{1}{100 \text{ ms}} \ln \left(\frac{\mu_+(100 \text{ ms})}{\mu_+(200 \text{ ms})} \right). \quad [38]$$

The rapid apparent relaxation rate and the saturation factors were then determined by fitting μ_+ by setting $T = f/(1 + f)$ with values of f taken from Ref. (4).

Transfer and difference term, apparent rates, and saturation factors were estimated by a global fit to all the data points. We applied a modified Levenberg-Marquardt routine without constraints as implemented in IDL 4.0.1 (Research Systems Inc., Boulder, CO). To simplify the partial derivations we assumed a monoexponential transition by μ_{+app} (Eq. [24]) toward the steady state M_f^∞/M_f^0 (Eq. [27]):

$$\begin{aligned} M_f^n(PR)/M_f^0 &= M_f^\infty(PR)/M_f^0 \\ &+ (1 - M_f^\infty(PR)/M_f^0)\mu_{+app}(PR)^n. \end{aligned} \quad [39]$$

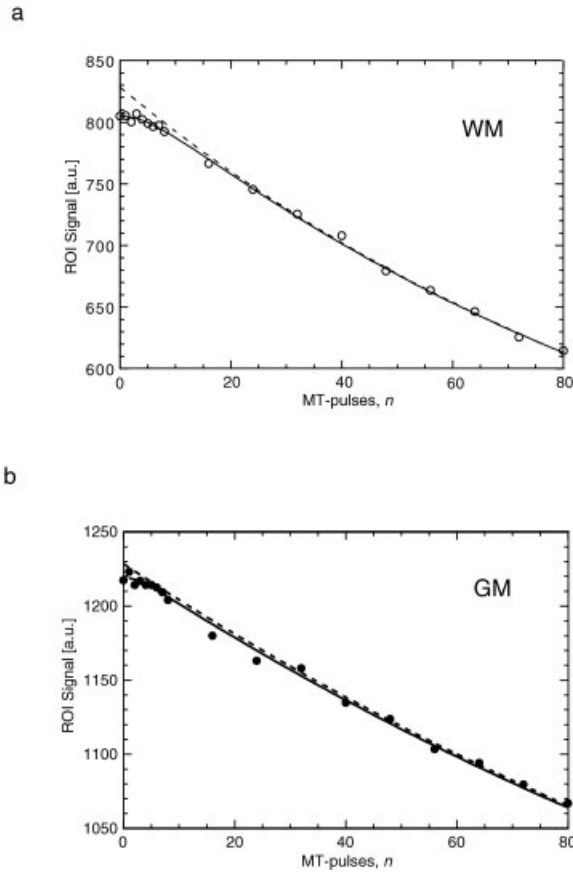


Figure 4 Biexponential transition observed in human WM (a) and GM (b). “Weak” Gaussian MT-pulses (3.2-ms duration, 180° flip angle, 4-kHz offset) and $PR = 5$ ms were used. Also shown is the fit of Eq. [11] (solid) and a monoexponential fit from which the first 20 pulses were left out.

RESULTS

Figure 4 shows the first 80 iterations of the transition for obtained at $PR = 5$ ms using the weak MT-pulses. The minor transient can be determined directly from a fit of Eq. [11] (solid line) or indirectly by comparison the reference signal to a monoexponential fit (dashed lines) excluding the points representing the first 20 iterations. The observed “overshoot” of the fitted amplitude was $2.6 \pm 0.4\%$ in WM and $0.6 \pm 0.4\%$ in GM. It was thus clearly exceeded than the residues in WM, where μ_+ was 0.9914 ± 0.0001 , and μ_- was 0.832 ± 0.042 . In GM, μ_+ was 0.9949 ± 0.0001 , and the error in μ_- was 80% (0.569 ± 0.455). In WM, η_f^1 was smaller than 0.001 but it could not be determined reliably by fitting Eq. [11] and was set to zero. The steady state saturation was $50.6 \pm 0.2\%$ in WM and $38.8 \pm 0.2\%$ in GM. In comparison, the monoexponential fit yielded higher steady state saturations. Thus, the minor transient may affect the evaluation,

although it proved too small to be suitable for quantitative evaluation.

The sharp decline towards 100% steady state saturation at very short PR could not be measured at either pulse length. For the “strong” MT-pulses of 12.8-ms duration, the minimum PR of 25 ms was too long. For the “weak” MT-pulses of 3.2-ms duration, the differential saturation was too small. Because the PR -dependence for weak MT-pulses resembles a homogeneous system, the steady state curve does not exhibit the distinctive bend that separates the regions of very short and short PR (see Fig. I-3). The use of strong MT-pulse appears to be the method of choice to evaluate the steady state.

After correction for CSF contributions and normalization, the steady state signal was consistently smaller in GM than in WM. An example is shown in Figure 5(a). Toward short PR , however, the GM and WM signals converged. This behavior corresponded to a slower apparent relaxation, but a smaller equilibrated saturation in GM than in WM (Table 1). The long PR range (≥ 100 ms) yielded λ_R and the equilibrated saturation (Eq. [I-41]). Nevertheless, it was not possible to determine all five parameters of Eq. [I-40] from the accessible range of PR . A probable explanation is that δ_f could not be determined reliably because very short PR s could not be measured. After replacing f with the values from Ref. (4), the other four parameters could be obtained. The fit returned consistent values for λ_R and the equilibrated saturation. The fitted values of λ_T were in most cases smaller than those given in Ref. (4).

When applying the 6.4-ms MT-pulses, the minor transition was not seen, so only the major transient was fitted. From $PR = 8$ ms to $PR = 200$ ms, the absolute error of the independently fitted μ_+ increased from 0.02% to 0.5%, as the steady state saturation decreased and the transition got shorter. Figure 5(b) shows the fitted PR -dependence of μ_{+app} in the ROIs of WM and GM. By means of Eq. [38] the slow apparent rate constant, λ_R , was determined to be 1.37 s^{-1} in WM and 0.87 s^{-1} in GM. Contrary to the steady state, the PR -dependence of μ_+ revealed clear differences between GM and WM, because the differences in λ_R and equilibrated saturation (3.3% in GM, 6.3% in WM) do not cancel each other. Contrary to the steady state, the PR -dependence of the transient can be extrapolated from short PR to zero without difficulty. Thus, the direct saturation can be determined with higher accuracy. Despite these advantages, the PR -dependence of μ_+ did not yield the complete set of parameters. The results obtained with fixed pool size ratios from (4) are given in Table 2.

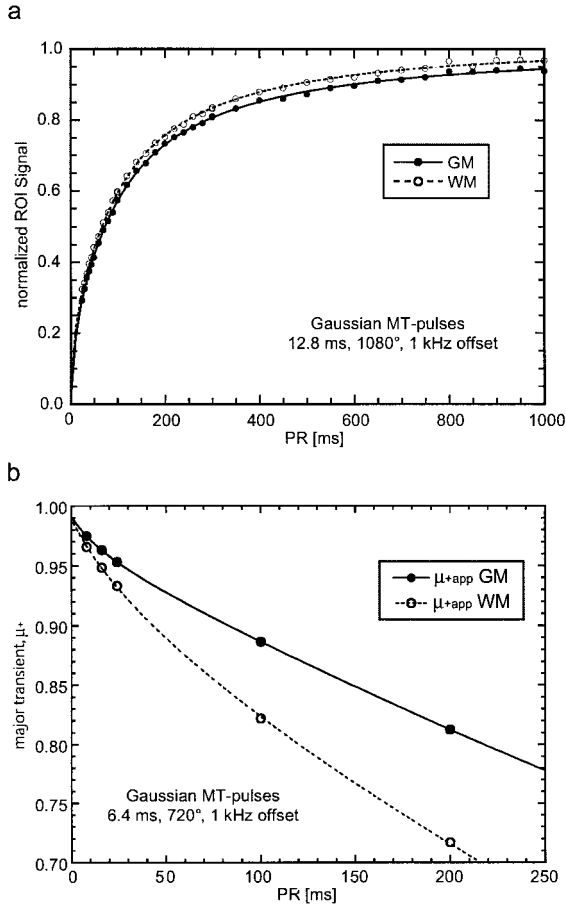


Figure 5 Fitting the PR -dependence of the normalized steady state signal (a) and of the major transient, μ_{+app} (b) Data from central WM (\circ) and GM (\bullet) was evaluated. The steady state signal was corrected for 1.3% CSF in WM and 17.6% CSF in GM. Strong Gaussian MT-pulses (12.8-ms duration, 1080° flip angle, 1-kHz offset) required a minimum PR of 25 ms. The fitted parameters are given in Table I. The transients were determined by independent mono-exponential fits to the data shown in Figure 6. Shorter MT-pulses of similar power (Gaussian shape, 6.4-ms duration, 720° flip angle, 1-kHz offset) were used. The fitted parameters are given in Table 2.

A quantification of the six system parameters was possible by a global least-squares fit to all data points, where the combined information from the transitions and the steady state was utilized. Figure 6 shows the data points and the curves, calculated from the parameters estimated by the global fit (Table 2). These correspond to rather large values of f (19.2% in WM, 9.4% in GM) and small k_{mf} (13.7 s^{-1} in WM, 20.3 s^{-1} in GM). The large value of D in WM yielded in $R_{1f} = 0.7 s^{-1}$ and $R_{1m} = 4.5 s^{-1}$. The global fit also reduced the errors of the parameter estimates. The parameters obtained from fitting the transients were consistent in WM, but not in GM. Reducing the number of parameters by setting $D = 0$, yielded consistent parameter estimates in GM, but not in WM. Only the macromolecular ratio was consistent in WM ($f = 18.5\%$), but it was larger in GM ($f = 12.1\%$). An F -test showed that the six-parameter fit yielded a significant improvement of the squared residues (χ^2) in WM, but not in GM.

DISCUSSION

This article presents the general analytic description of the dynamic behavior of a two-pool system under linear exchange and arbitrary instantaneous saturation. The results are applied to describe MT in brain tissue. The transition of the free water may be delayed by a small second component. However, the key finding is that the typical MT-experiment can be described by analogy to partial progressive saturation by means of a PR -dependent apparent saturation. A complete quantification of the system can be obtained by sampling the transient behavior at various PR .

The second component of the free water signal may be observed in the first iterations only if PR is short and the MT-pulse is weak. Under these conditions, the individual saturations, δ_f and δ_m , can be obtained by extrapolation of μ_+ and μ_- to $PR = 0$,

Table 1 Slow Apparent Relaxation Rate and Saturation Factors Fitted to Steady State Signal in Figure 5(a)

	WM ^a	WM ^b	GM ^a	GM ^b
	0.025 s $\leq PR \leq$ 1 s	0.1 s $\leq PR \leq$ 1 s	0.025 s $\leq PR \leq$ 1 s	0.1 s $\leq PR \leq$ 1 s
λ_R (s^{-1})	1.44 \pm 0.05 (3%)	1.39 \pm 0.08 (5%)	0.51 \pm 0.06 (12%)	0.52 \pm 0.06 (11%)
λ_T (s^{-1})	36.8 \pm 5.1 (14%)	—	43.4 \pm 4.8 (11%)	—
δ_f (%) ^c	2.6 \pm 1.0 (38%)	—	0.3 \pm 0.4 (133%)	—
δ_m (%) ^c	79.1 \pm 6.1 (8%)	—	94.5 \pm 8.8 (9%)	—
$\delta_f + T(\delta_m - \delta_f)$ (%) ^c	9.9	10.3 \pm 0.6 (6%)	3.6	4.0 \pm 0.5 (13%)

Duration of MT-pulses: 12.8 ms, offset 1 kHz, nominal flip angle 1080°.

^a Four parameter fit of Eq. [I-40] to the whole PR range using $f = 10.6\%$ for WM and 3.7% for GM (4).

^b Two parameter fit of Eq. [I-40] to the range of long PR .

^c Calculated with $T = f/(1 + f)$ with values of f taken from Ref. (4).

Table 2 Apparent Relaxation Rates and Saturation Factors Determined by Fitting the PR Dependence of μ_{+app} (Eq. [24])

	WM μ_{app+}	WM Global	WM Global	GM μ_{app+}	GM Global	GM Global
λ_R (s^{-1})	1.37 ^a	1.31 ± 0.01	0.96 ± 0.02	0.87 ^a	0.74 ± 0.05	0.70 ± 0.05
λ_T (s^{-1})	20.7 ± 5.4	20.2 ± 0.6	30.1 ± 0.7	45.3 ± 1.7	23.7 ± 2.7	23.4 ± 2.8
δ_f (%)	1.4 ± 0.2	0.9 ± 0.1	0.4 ± 0.01	0.9 ± 0.1	0.8 ± 0.1	0.7 ± 0.1
δ_m (%)	52.3 ± 3.2	50.4 ± 0.1	37.2 ± 0.1	67.9 ± 1.0	45.8 ± 3.8	40.0 ± 3.2
T (%)	9.6 ^b	10.6 ± 0.05	15.6 ± 0.6	3.6 ^b	7.9 ± 0.5	9.5 ± 0.6
D (%)	0 ^c	-3.2 ± 0.1	0 ^c	0 ^c	-0.3 ± 0.3	0 ^c

Transfer and difference terms were determined by a global fit of a single transient, μ_{+app} , using Eq. [40].

^a Determined from μ_{+} at $PR = 100$ ms and $PR = 200$ ms by means of Eq. [38].

^b Approximation with $T = f/(1 + f)$. The values for f were taken from Ref. (4).

^c $D = 0$ was implied by the approximations of fast exchange and small f .

respectively. However, the transfer and difference terms are difficult to determine from Eqs. [24] and [26], because the differential saturation ($\delta_m - \delta_f$) is small. The small amplitude of the minor component impedes quantification. The origin of the minor transition is the additional saturation of the macromolecular pool that results from incomplete MT at short PR . When this saturation is built up during the first iterations of the MT-pulse train, it delays the progressive saturation of the free pool. Afterwards, the two pools slowly approach the steady state together. Saturation by a pulse train at short PR is thus fundamentally different from a model proposed by Eng et al. (6) for partial CW saturation, where the macromolecular pool instantaneously assumes its steady state.

A strong macromolecular saturation is beneficial in order to estimate the kinetic rates from transfer and difference term: This suppresses the minor transient, increases the amount of transferred saturation, and thus helps to determine T and λ_T . Although the steady state and the major transient provide theoretically the same information about MT (when $D = 0$), fitting the PR -dependence of μ_{+} is more robust to errors. This applies in particular to the exponential dependence of μ_{+} at long PR , whereas fitting λ_R to the steady state depends on system stability and accurate determination of the reference signal. Errors in λ_R will in turn affect the contributions from the rapid apparent rate. In addition, the differences in relaxation and smaller transfer term cancel in the steady state, but amplify each other in the major transient (Fig. 5).

Because the macromolecular ratio could not be determined from the PR -dependence of the steady state without prior knowledge (and likewise for the major transient), a global fit is needed for quantification. At least one long PR should be measured to yield λ_R and the equilibrated saturation, $\delta_f + T(\delta_m - \delta_f)$. The whole range of short PR should be sampled (from

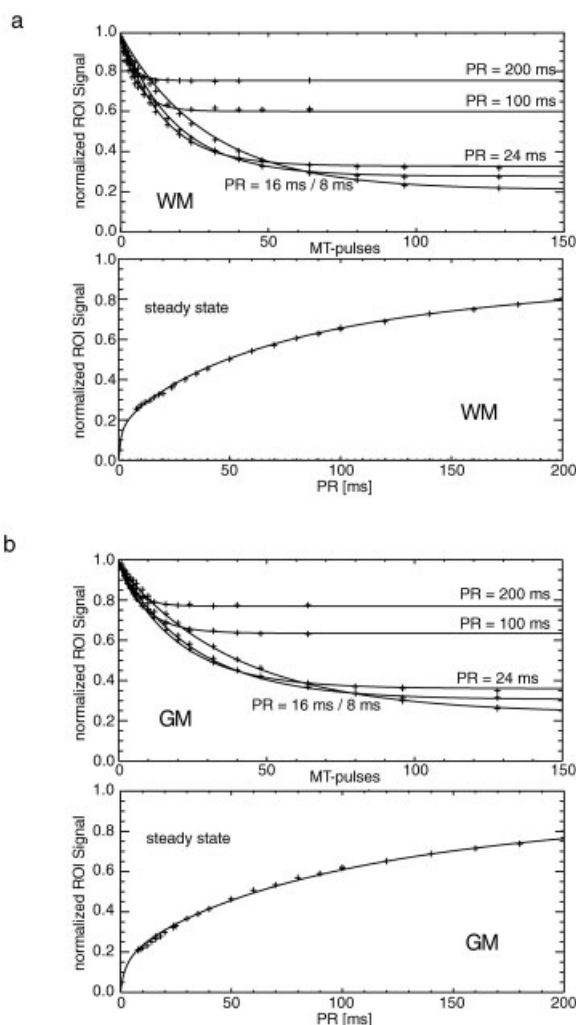


Figure 6 Global fit of the transient behavior in WM (a) and GM (b). Five transitions with were fitted using μ_{app+} (top panels). In addition, the steady state was sampled at PR between 8 ms and 200 ms (bottom panels). Note that the steady state is reached after fewer MT-pulses as the transient gets shorter for larger PR .

t_{crit} to the minimum PR) to yield λ_T , T , δ_m . This however increases the time requirement of the experiment. The global fit combines transient and steady state, which both depend on the transfer term, T . D is thus determined from the mismatch between transient and steady state at long PR . However, the evaluation of small amplitude changes (as for example, D , small MTR, and the amplitude of the second component) may fail when they are of the same size as the error due to noise, scanner instability, and subject motion. Partial volume contributions from adjacent structures containing CSF also increase the susceptibility to subject motion. The quantitative evaluation is strongly influenced by the CSF signal. This should be determined by an independent T_2 -measurement, but the CSF component is still subject to minor attenuation by progressive saturation and MT (7). For a more robust evaluation, the number of fitted parameters can be reduced to five by $D = 0$ (or $R_{1f} = R_{1m} = \lambda_R$). The transfer term then equals the macromolecular fraction, $f/(1 + f)$. In GM, increased errors of the global fit and the inconsistencies with the μ_+ fit indicate signal variations during the course of the experiment. Measurements of the reference signal at regular intervals are recommended.

The direct saturation is estimated with high accuracy from the major transient if the sampled PR 's are sufficiently short. Contrary to our earlier suggestion (8), direct saturation must not be neglected in the major transient, because μ_+ can be determined with an accuracy far better than 1%. Although the expressions simplify considerably when $\delta_f = 0$, this affects the extrapolation to zero PR , which will result in an overestimation of the transfer term. The approximation given by $\mu_{\text{-app}}$ and $\mu_{\text{+app}}$ appears to be a reasonable compromise of simplification and exactness. The fast-transfer approximation appears to be valid for the whole range of δ_m and PR achievable on whole body MR systems. In combination with a small pool size ratio, this amounts to the assumption of one common relaxation rate, which roughly corresponds to equating R_{1m} to one (4, 9–12). This is especially helpful for a qualitative understanding of the mechanism of MT. The equal-relaxation approximation provided the most robust fits when evaluating steady state and transition separately. When the inconsistency between major transient and steady state is to be exploited to reveal difference between R_{1f} and R_{1m} by global fitting, this approximation may not be applied.

So far, only one study has exploited the transition for quantitative MT (12). The inverse MT effect can also be utilized by measuring one transition to steady state in a multiple inversion experiment (2). At a long PR , this yields the apparent relaxation rate and the

equilibrated saturation (Eq. [I-42]), from which the pool size ratio can be derived if the saturations are known (2). In the presence of an unknown amount of CSF, these values can be derived from two measurements of the transient (Eq. [38]) because the transient is not directly affected by CSF contributions. In addition, the transient can be determined with high accuracy because a major part of the transition needs to be sampled without actually reaching the steady state.

Previously, quantitative studies of the kinetic and relaxation properties in human brain have been performed in the steady state, by varying the frequency offset and power of the radio-frequency irradiation for constant PR (9–11). In this study, we varied PR , rather than the MT-pulse. The backward rate constant, k_{mf} , was smaller than found in Refs. (4, 9–11). Accordingly, the macromolecular ratio was quite large (especially in GM). In WM, this may be due to the slow exchange of myelin-water of short T_2 . Myelin water mediates most of the MT effect (13) and is subject to direct saturation, but it is unobservable at $TE = 50$ ms. Exchange effects on MT have been observed in vivo for delays up to 200 ms (14). Including the difference term into the fit resulted in a significant reduction of the χ^2 sum for WM, but a larger value of D than predicted by (4) (Table 1 in part I). The difference term had a strong influence on the calculation of the primary parameters k_{fm} , k_{mf} , R_{1f} , R_{1m} . The rapid relaxation of the macromolecular pool in WM is consistent with the hypothesis that part of the myelin water is contributing to this pool. The absence of partial volume contributions from CSF in the WM ROI, small errors, and lack of consistency when assuming $D = 0$ support the notion that these findings reflect properties of WM.

SUMMARY

The evolution of two pools of magnetization undergoing periodic pulsed saturation for magnetization transfer experiments can be analytically solved. The transition to steady state is especially useful for quantitative evaluation of in vivo MT experiments: it is little affected by partial CSF volume; its major component, μ_+ , can be determined with high accuracy. When compared to the steady state, the PR -dependence of μ_+ could be fitted more robustly. Quantification of all system parameters is possible by a global fit of several transitions at several PR covering the short PR -domain.

APPENDIX

f subscript, denoting the pool of free or bulk water
 m subscript, denoting the pool of macromolecules
 M_f, M_f^0 longitudinal magnetization of free water, equilibrium value
 M_m, M_m^0 longitudinal magnetization of macromolecules, equilibrium value
 $f = M_m^0/M_f^0$ pool size ratio, defined in Eq. [I-1]
 η_f, η_m fractional reduction of longitudinal magnetization = saturation, defined in Eq. [I-2a,b]
 $\boldsymbol{\eta} = (\eta_f, \eta_m)^T$ column vector of saturations
 $T, -1$ superscripts to matrices, denoting transposition and inversion
 R_{1f}, R_{1m} rates of longitudinal relaxation
 k_{fm}, k_{mf} kinetic rate constants of forward ($f \rightarrow m$) and backward ($m \rightarrow f$) transfer
 $R_f = R_{1f} + k_{fm}, R_m = R_{1m} + k_{mf}$ combined rates of relaxation and transfer; defined in Eq. [I-4a,b]
 λ_R, λ_T apparent rates of Relaxation and Transfer as observed in the evolution when no RF is irradiated, e.g. after pulsed saturation, defined in Eq. [I-7a,b]
 E_R, E_T the corresponding decaying exponentials
 t, PR time, repetition period of MT pulses
 \mathbf{T} 2×2 transfer matrix, defined in Eq. [I-9]
 $T_{ff}, T_{fm}, T_{mf}, T_{mm}$ elements of transfer matrix, the first subscript denotes the observed pool, the second the saturated pool (Eqs. [I-14,15])
 I 2×2 unity matrix
 t_{crit} “critical” time delay providing the largest transferred saturation, i.e., the maximum in $E_R - E_T$, Eq. [I-12]
 T Transfer term, defined in Eq. [I-15], parameterizes \mathbf{T} in Eq. [I-18]
 D Difference term, defined in Eq. [I-16], parameterizes \mathbf{T} in Eq. [I-18]
 δ_f, δ_m degree of saturation caused by one MT-pulse on free water and macromolecules (‘direct’ and ‘macromolecular’ saturation), defined in Eq. [I-25]
 $\delta_{f \text{ app}}$ apparent saturation, defined in Eq. [I-41]
 n superscript to $\boldsymbol{\eta}$, denotes the number of iterated MT-pulses
 ∞ superscript to $\boldsymbol{\eta}$, denotes the steady state
 $-, +$ superscripts to $\boldsymbol{\eta}$, denote the steady state before and after an MT-pulse
 $g(\omega)$ absorption line shape of macromolecular pool
 $B_1(t)$ time varying amplitude of RF pulse
 \mathbf{A} matrix in the recursion for $\boldsymbol{\eta}^n$, defined in Eq. [II-2]
 \mathbf{b} matrix in the recursion for $\boldsymbol{\eta}^n$, defined in Eq. [II-3]
 μ_+, μ_- “major” and “minor” transients, eigenvalues of \mathbf{A} , defined in Eq. [II-8]
 $\mu_{\text{-app}}$ approximation of the minor transient, defined in Eq. [II-23]

$\mu_{\text{+app}}$ approximation of the minor transient, defined in Eq. [II-24]

$\Delta \boldsymbol{\eta}^n = \boldsymbol{\eta}^n - \boldsymbol{\eta}^{n-1}$ increase in saturation between MT-pulse $n - 1$ and n

ACKNOWLEDGMENTS

Major parts of this work were done while on leave from the Karolinska Institute. The general solution was derived during a research visit to the Max-Planck-Institute in Göttingen. Experiments were performed at the Santa Lucia Foundation in Rome. The hospitality of the Functional Neuroimaging lab is gratefully acknowledged.

REFERENCES

1. Wolff SD, Balaban RS. 1989. Magnetization transfer contrast (MTC) and tissue water proton relaxation in vivo. *Magn Reson Med* 10:135–144.
2. Gochberg DF, Kennan RP, Robson MD, Gore JC. 1999. Quantitative imaging of magnetization transfer using multiple selective pulses. *Magn Reson Med* 41:1065–1072.
3. Listerud J. 1997. Off-resonance pulsed magnetization transfer in clinical MR imaging: Optimization by an analysis of transients. *Magn Reson Med* 37:693–705.
4. Graham SJ, Henkelman RM. 1999. Pulsed magnetization transfer imaging: evaluation of technique. *Radiology* 212:903–910.
5. Helms G, Frahm J. 1999. Magnetization transfer attenuation of creatine resonances in localized proton MRS of human brain in vivo. *NMR Biomed* 12:490–494.
6. Eng J, Checkler TL, Balaban RS. 1991. Quantitative ^1H magnetization transfer imaging in vivo. *Magn Reson Med* 17:304–314.
7. Helms G, Piringner A. 2001. Magnetization transfer of water T_2 relaxation components in human brain: Implications for T_2 -based segmentation of spectroscopic volumes. *Magn Reson Imaging* 19:803–811.
8. Helms G, Piringner A. 1998. Dynamic evaluation of magnetization transfer (MT) in human brain: The approach to steady state after pulsed saturation. In: *Book of Abstracts, 6th Annual Meeting of the Int'l Society for Magnetic Resonance in Medicine*. Berkeley CA: ISMRM, p 2192.
9. Sled JG, Pike GB. 2001. Quantitative imaging of magnetization transfer properties in vivo using MRI. *Magn Reson Med* 46:923–931.
10. Yarnykh VL. 2002. Pulsed Z-spectroscopic imaging of cross-relaxation parameters in tissues for human MRI: Theory and clinical applications. *Magn Reson Med* 47:929–939.
11. Ramani A, Dalton C, Miller DH, Tofts PS, Barker GJ. 2002. Precise estimate of fundamental in vivo MT parameters in human brain in clinically feasible times. *Magn Reson Imaging* 20:721–731.

12. Chai J-W, Chen C, Chen JH, Lee S-K, Yeung HN. 1996. Estimation of in vivo proton intrinsic and cross-relaxation rates in human brain. *Magn Reson Med* 36:147–152.
13. Stanisz GJ, Kecojevic A, Bronskill MJ, Henkelman RM. 1999. Characterizing white matter with magnetization transfer and T_2 . *Magn Reson Med* 42:1128–1136.
14. Vavasour IM, Whittall KP, Li DKB, MacKay AL. 2000. Different magnetization transfer effects exhibited by the short and long T_2 components in human brain. *Magn Reson Med* 44:860–866.

BIOGRAPHY



Gunther Helms is research physicist at the University Hospital in Tübingen, Germany, and associate professor in MR physics at the Karolinska Institute in Stockholm. He received his basic training at the University of Göttingen and his PhD working with Prof. J. Frahm at the Max-Planck-Institute for Biophysical Chemistry. His scientific interests

involve clinical spectroscopy and quantification methods.



Henning Dathe is a jazz guitarist and senior research physicist at the Biomechanics Research Group at the University of Göttingen, Germany. He was trained in theoretical physics at the University of Göttingen, and received his PhD working on a general theoretical framework for elastically suspended rigid bodies. His research interests involve the application of differential geometry to

biomechanical problems.



Gisela E. Hagberg is senior research physicist at the Santa Lucia Foundation in Rome since 1999. She got her physics training at the Institute of Technology, in Lund, Sweden and in Lausanne, Switzerland, and obtained a PhD in Biophysics at the University of Basel in 1993 working with ^1H -MRS of the human brain in the group of Prof. J. Seelig. Her scientific in-

terests are structural and functional MR-applications in the field of the neurosciences.